A New Negative-Sequence Cross-Differential Algorithm for Double-Circuit Line Protection

César C. S. Silva, Vitor R. Serpa, Kleber M. Silva

***Abstract*—This paper proposes a new alpha plane-based negative-sequence cross-differential protection algorithm for double-circuit transmission lines. To demonstrate its usefulness, the algorithm's performance was evaluated through faults simulated in a 230 kV, 200 km long double-circuit transmission line using ATPDraw. The results reveal that the proposed algorithm provides a reliable and fast operation for asymmetric faults on both circuits of the line, as well as ensuring security for external faults, revealing it as a promising alternative for improving double-circuit transmission line protection.**

***Keywords*—Alpha-Plane, Cross-Differential Protection, Double-Circuit Transmission Lines, Negative Sequence.**

I. Introduction

DOUBLE-circuit transmission lines are frequently used in high-voltage systems due to their greater power transfer capacity and the possibility to share the same tower or right-of-way [1]. Notwithstanding, proximity between circuits results in mutual coupling between them, which can jeopardize traditional protection elements performance. Although line transposition schemes can significantly reduce positive- and negative-sequence coupling, zero-sequence coupling remains quite significant as it accounts for 50% to 70% of the self-impedance of each line [2].

Typically, unit protection for double-circuit lines uses longitudinal differential elements and other pilot schemes. However, communication channel availability is critical, since both protection schemes are taken out of service if communication is lost, prevailing backup non-unit underreaching elements [1]. Furthermore, as longitudinal differential schemes require data synchronization, complexity and costs are increased as a whole. On the other hand, cross-differential protection has been reported in the literature as a promising alternative to enhance double-circuit transmission line protection, since it uses currents measured at the same terminal of both circuits, being independent of communication between line terminals or data synchronization [2]–[4].

Several papers have evaluated cross-differential protection, but none of them have proposed an algorithm that exploits negative-sequence components. These existing algorithms have been shown to work correctly. However, some studies have tested their performance in transmission lines with series compensators, which can introduce errors due to subsynchronous resonance. Therefore, this paper proposes an alpha plane-based cross-differential protection scheme, where the negative-sequence current ratio is calculated for each circuit using currents measured at the same terminal. Negative-sequence currents inherently present incremental behavior, and are immune to load currents. Moreover, the influence of zero-sequence coupling between circuits on protection performance is eliminated, as such a component is removed during the negative-sequence components calculation. Although the proposed algorithm does not operate for symmetrical faults, it can serve as a complementary logic within the protection system, enhancing fault detection in specific scenarios.

This study was financed in part by the Coordination for the Improvement of Higher Education Personnel (CAPES) and the Brazilian National Council for Scientific and Technological Development (CNPq).

César Silva, Vitor Serpa and Kleber Melo are with the Department of Electrical Engineering at University of Brasília, Brasília, Federal District, Brazil. (e-mail: [cesar.carlyle, vitorserpa]@lapse.unb.br, klebermelo@unb.br)

Paper submitted to the International Conference on Power Systems Transients (IPST2025) in Guadalajara, Mexico, June 8-12, 2025.

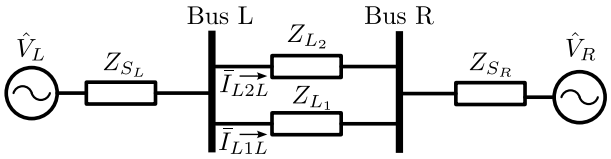

Fig. 1: Cross-differential protection overview.

II. Cross-Differential Protection Fundamentals

According to cross-differential protection (87LT) principles, a percentage differential element can be used with currents measured in both circuits at the same line terminal [5], as presented in Fig. 1.

Thus, for the percentage cross-differential element, equations for operating and restraining currents are defined by (1) for circuit 1 element and by (2) for circuit 2 element [5]:

$$I_{op} = |\bar{I}_{L1L}| - |\bar{I}_{L2L}|, \qquad I_{res} = |\bar{I}_{L1L}| + |\bar{I}_{L2L}|, \quad (1)$$

$$I_{op} = |\bar{I}_{L2L}| - |\bar{I}_{L1L}|, \qquad I_{res} = |\bar{I}_{L2L}| + |\bar{I}_{L1L}|, \quad (2)$$

in which I_{op} is the operating current and I_{res} is the restraining current. Furthermore, $\bar{I}_{L1L}$ and $\bar{I}_{L2L}$ represent the current phasors measured by the current transformers of circuits 1 and 2 at the local terminal, respectively. In (1) and (2), the operating and restraining currents are defined per phase. Consequently, for each element of circuit 1, there are three operating currents and three restraining currents, corresponding to phases A, B, and C. Similarly, for circuit 2, three operating and three restraining currents are also considered, ensuring that the protection scheme analyzes each phase independently.

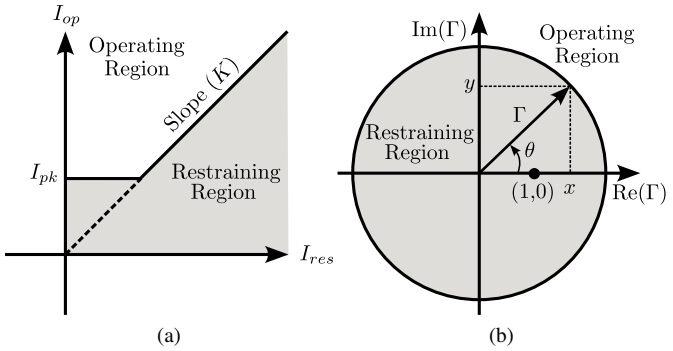

Fig. 2: Representation planes: (a) The $I_{op} \times I_{res}$ Plane and (b) Alpha-Plane.

A. The $I_{op} \times I_{res}$ Plane

In $I_{op} \times I_{res}$ plane, illustrated in Fig. 2a, the abscissa axis represents I_{res}, and the ordinate axis represents I_{op}. This plot divides the plane into two regions: the restraining region (gray region), which lies below the line formed by the pick-up current (I_{pk}) and the adjustable curve as a function of the restraining current; the operating region, which lies above this line (white region). When the I_{op} settles within the operating region, the relay will act by issuing a trip command to the circuit breakers. The protection sensitivity can be adjusted by the slope setting (K), with a steeper curve leading to a less sensitive protection element. The 87LT function will issue a trip command if both conditions are met:

$$I_{op} > I_{pk}, \tag{3}$$

$$I_{op} > K I_{res}. \tag{4}$$

B. Alpha-Plane

The Alpha-Plane is a complex representation where the coordinate axes represent the real and imaginary parts of the ratio Γ. In 87LT protection element, the ratio is calculated using the currents ratio ($\bar{I}_{L1L}/\bar{I}_{L2L}$) for circuit 1 protection, as presented in (5) [6], [7].

$$\Gamma = \frac{\bar{I}_{L1L}}{\bar{I}_{L2L}} = x + jy = |\Gamma| e^{j\theta}, \tag{5}$$

in which magnitude is given by:

$$\frac{|\bar{I}_{L1L}|}{|\bar{I}_{L2L}|} = |\Gamma| = \sqrt{x^2 + y^2}, \tag{6}$$

and phase is given by: $\theta = \arctan\left(\frac{y}{x}\right)$, where $x = |\Gamma|\cos(\theta)$ and $y = |\Gamma|\sin(\theta)$. Similarly, the ratio can be calculated using the current ratios ($\bar{I}_{L2L}/\bar{I}_{L1L}$) for circuit 2 protection.

This representation is depicted in Fig. 2b and allows improving relay operation accuracy during transmission system disturbances [6].

The cross-differential protection calculates the ratio Γ from the current modulus of circuits 1 and 2 at the same terminal. During steady state, before fault takes place, the alpha-plane ratios are located at point $(1, 0)$. For internal faults, the ratios must lie outside the restraining region, defined by the circle, as shown in Figure 2b.

The alpha-plane uses a mapping strategy by means of equations. The protection element issues a trip command whenever I_{op} exceeds a certain percentage K of the restraining current, as presented in (1) and (4).

From these equations, we obtain the operating limit, as:

$$|\bar{I}_{L1L}| - |\bar{I}_{L2L}| = K(|\bar{I}_{L1L}| + |\bar{I}_{L2L}|), \tag{7}$$

by dividing each side of (7) by $|\bar{I}_{L2L}|$, we get:

$$\frac{|\bar{I}_{L1L}|}{|\bar{I}_{L2L}|} - 1 = K\left(\frac{|\bar{I}_{L1L}|}{|\bar{I}_{L2L}|} + 1\right), \tag{8}$$

Since the ratio of magnitudes of the currents is numerically equal to the magnitude of the ratio of these currents, we have:

$$(1 - K)\left|\frac{\bar{I}_{L1L}}{\bar{I}_{L2L}}\right| = (1 + K). \tag{9}$$

Isolating the term $\bar{I}_{L1L}/\bar{I}_{L2L}$ in (9), we obtain:

$$\left|\frac{\bar{I}_{L1L}}{\bar{I}_{L2L}}\right| = \frac{1+K}{1-K}, \tag{10}$$

$$\sqrt{x^2 + y^2} = \frac{1+K}{1-K}, \tag{11}$$

$$x^2 + y^2 = \left(\frac{1+K}{1-K}\right)^2. \tag{12}$$

Thus, the operating region for circuit 1 is defined by the area outside a circle with radius $\frac{1+K}{1-K}$, centered at $(0, 0)$ [8].

III. Negative-Sequence Cross-Differential Protection

Likewise conventional 87LT, the operating current (I_{opQ}) and restraining current (I_{resQ}) of the negative-sequence cross-differential protection element (87LTQ) for circuit 1 are given by:

$$I_{op1Q} = |\bar{I}_{L1q}| - |\bar{I}_{L2q}|, \tag{13}$$

$$I_{res1Q} = |\bar{I}_{L1q}| + |\bar{I}_{L2q}|. \tag{14}$$

in which negative-sequence current is calculated by $\bar{I}_{Lnq} = \frac{1}{3}\left(\bar{I}_{Lna} + a^2\bar{I}_{Lnb} + a\bar{I}_{Lnc}\right)$, where $a = 1\angle 120°$ and $n = 1, 2$, depending on the analyzed circuit [9].

The 87LTQ element used in this paper is defined as (5) for protection in the local bus:

$$\Gamma_{1Q} = \frac{\bar{I}_{L1q}}{\bar{I}_{L2q}}. \tag{15}$$

When we analyze the negative-sequence circuit in Fig. 3, h represents the percentage of the circuit 1 where faults are applied, starting from local terminal (see Fig. 3). Z_{L1} is the impedance of circuit 1 and Z_{L2} is the impedance of circuit 2. The subscript q indicates that the impedances are related to the negative-sequence. The current $\bar{I}_2$ represents the negative-sequence current arising due to the contribution of the system's negative-sequence network at the fault point. This current can be determined based on the type of asymmetrical fault and the circuit topology. It can be calculated if the fault currents in each phase at the fault point are known, using [9].

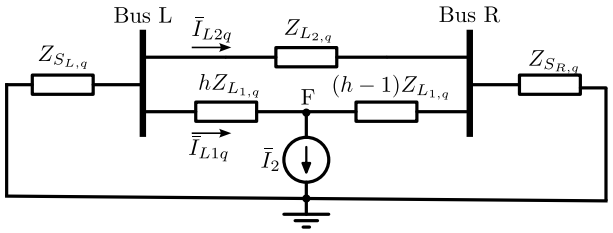

Fig. 3: Negative-Sequence Circuit.

After mathematical manipulations, which involve solving a 3×3 system of equations through substitution, it is possible to find the current values of $\bar{I}_{L1q}$, $\bar{I}_{L2q}$ and the negative-sequence current of circuit 1, which originates from the remote bus and flows toward the fault point (F), as a function of the circuit impedances, h, and $\bar{I}_2$, considering circuit 1 impedance equals to circuit 2 impedance (*i.e.,* $Z_{L_q} = Z_{L_{1,q}} = Z_{L_{2,q}}$):

$$\bar{I}_{L1q} = \frac{\bar{I}_2 \left[Z_{L_q} + Z_{S_{L,q}} + 2Z_{S_{R,q}} - h\left(Z_{L_2} + Z_{S_{L,q}} + Z_{S_{R,q}}\right)\right]}{Z_{L_q} + 2Z_{S_{L,q}} + 2Z_{S_{R,q}}}, \tag{16}$$

$$\bar{I}_{L2q} = \frac{\bar{I}_2 \left[-Z_{S_{L,q}} + h\left(Z_{S_{L,q}} + Z_{S_{R,q}}\right)\right]}{Z_{L_q} + 2Z_{S_{L,q}} + 2Z_{S_{R,q}}}. \tag{17}$$

It is possible to calculate the ratio in the alpha-plane:

$$\Gamma_{1Q} = \frac{Z_{L_q} + Z_{S_{L,q}} + 2Z_{S_{R,q}} - h\left(Z_{L_2} + Z_{S_{L,q}} + Z_{S_{R,q}}\right)}{-Z_{S_{L,q}} + h\left(Z_{S_{L,q}} + Z_{S_{R,q}}\right)}. \tag{18}$$

It is noteworthy to point out that this protection element does not depend on fault resistance or fault type, except for symmetrical faults, which do not have a negative sequence current so the proposed function does not operate. Note from Fig. 3 that the line was considered using the short-line model. Moreover, since negative sequence arises for any assymetrical faults, it is necessary to employ a faulted phase selection whenever single pole tripping is required. Nevertheless, this is not a drawback, since this is a kind of additional logic employed on IEDs readily available on the market.

Considering the use of the exact pi model for the transmission line, an additional component would be introduced due to the capacitive current, making it necessary to recalculate the parameters for a more complex system. However, a simplification was adopted by using the short-line model. Nevertheless, tests were conducted, and similar behaviors were observed, such as circular arcing. The results show convergence for faults located further from the analyzed terminal, while for faults closer to the terminal, a slight discrepancy is observed.

Even though more elaborate definitions to source impedance ratio (SIR) for double circuit lines are reported in the literature [10], for the sake of simplicity, here we consider it as:

$$\text{SIR}_{L,q} = \frac{2Z_{S_{L,q}}}{Z_{L_q}}, \quad \text{SIR}_{R,q} = \frac{2Z_{S_{R,q}}}{Z_{L_q}}. \tag{19}$$

Thus, we can simplify the equation that defines the ratio in the alpha-plane by factoring Z_{L_q} in both the numerator and the denominator:

$$\Gamma_{1Q} = \frac{2 + \text{SIR}_{L,q} + 2\ \text{SIR}_{R,q} - h\left(2 + \text{SIR}_{L,q} + \text{SIR}_{R,q}\right)}{-\text{SIR}_{L,q} + h\left(\text{SIR}_{L,q} + \text{SIR}_{R,q}\right)} \tag{20}$$

IV. Simulation and Experimental Results

The ATPDraw test model consisted of a 230 kV system with a 200 km long double-circuit line. The system and proposed function parameters are available in Table I. It is worth mentioning that a complex $\text{SIR}_{R,q}$ was used to take into account the inhomogeneous characteristic of the system.

TABLE I: Selected Parameters.

Parameter	Value
K	0.3
I_{pkQ}	200 A primary
$\text{SIR}_{L,q}$	0.1

A. Fault Trajectories

The fault trajectories analysis consisted of evaluating the protection performance under fault conditions in steady state, considering fault and system parameters variation as shown in Table II. Therefore, three cases of this kind of analysis are presented in Fig. 4, aiming to reveal the behavior of the proposed algorithm with variation in $\text{SIR}_{R,q}$.

TABLE II: Simulated Fault Scenarios.

Case	h (%)	$\text{SIR}_{L,q}$	$\lvert\text{SIR}_{R,q}\rvert^*$
1	varied	0.1	1.0
2	varied	0.1	0.5
3	varied	0.1	0.05

Legend:
* Considering $\arg(\text{SIR}_{L,q}) = 0^\circ$ and $\arg(\text{SIR}_{R,q}) = [-20^\circ, 0^\circ \text{ or } 20^\circ]$.

The calculated values were determined by varying fault location (h) between 1% and 99%, in steps of 0.3%.

The value of $SIR_{L,q}$ was set to 0.1 to ensure that variations between strong and weak remote sources could be observed within the same scale. Choosing a different value could lead to abrupt variations with changes in the remote source strength, making the analysis less consistent.

The magnitude of $SIR_{R,q}$ is related to the source strength, while its angle was introduced to represent different relationships between resistance and reactance in the equivalent source impedance. The values of -20° and 20° were chosen as practical limits based on real-system tests, where exceeding these boundaries could lead to negative resistance, which is not physically viable. The 0° case represents a homogeneous system.

In Figure 4a, three trajectories are presented, in which blue curve represents the $\text{SIR}_{R,q} = 1.0\angle{-20^\circ}$, green curve represents the $\text{SIR}_{R,q} = 1.0\angle{0^\circ}$ (ideally homogeneous system), and red curve represents the $\text{SIR}_{R,q} = 1.0\angle{20^\circ}$. When the fault occurs close to the local bus, the starting point of the curves is near the x-axis at (-45, 0). As the values of h increase, two types of occurrences arise. Initially, the $\text{SIR}_{R,q}$ equal to $1.0\angle{-20^\circ}$ and $1.0\angle{20^\circ}$ will trace a circular arc towards the point (1,0), while the green curve ($\text{SIR}_{R,q} = 1.0\angle{0^\circ}$) will tend to infinity and return in the other half-plane. Another curious fact is that when both local

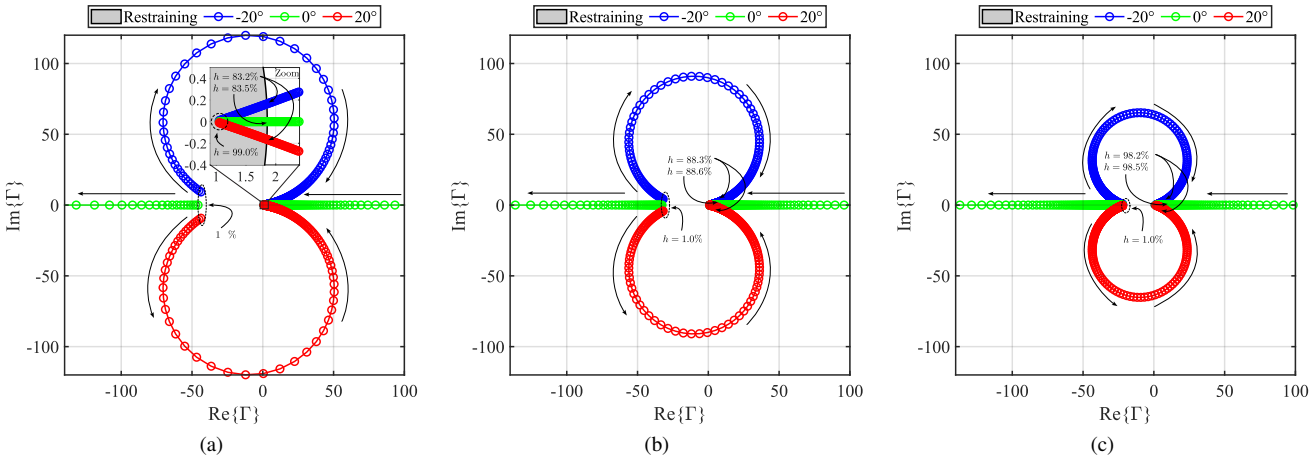

Fig. 4: Trajectories of Faults for variation in the $|\text{SIR}_R|$: (a) 1.0, (b) 0.5 and (c) 0.05.

and remote SIR are real (*i.e.,* the system is considered ideally homogenous), the value of Γ_{1Q} will also have only a real part.

Note that for the cases of $\text{SIR}_{R,q}$ equal to $1.0\angle{-20°}$ and $1.0\angle{20°}$ with faults between 83.2% and 99% of the transmission line, the 87LTQ algorithm remains within the restraining region, indicating that there is no operation for faults within this interval. As a result, in these cases, the function would have an operational coverage of 83.2%. However, for an instantaneous operating zone of the 87LTQ function, it is necessary for both terminals, local and remote, to operate simultaneously, resulting in an instantaneous coverage of 66.4% of the line. In the case of $\text{SIR}_{R,q} = 1.0\angle{0°}$, there is a small increase in coverage, reaching 83.5%, with the instantaneous coverage corresponding to 67% of the line.

The same happens for Figure 4b, in which $|\text{SIR}_{R,q}| = 0.5$, indicating an increase in remote source strength. A decrease in trajectories radius formed by the elements in $\text{SIR}_{R,q}$ equal to $0.5\angle{-20°}$ and $0.5\angle{20°}$ was observed. Additionally, an increase in the line coverage was noted, rising to 88.3% (equivalent to an instantaneous coverage of 76.6%) for $\text{SIR}_{R,q}$ equal to $0.5\angle{-20°}$ and $0.5\angle{20°}$, and 88.6% (instantaneous coverage of 77.2%) for $\text{SIR}_{R,q} = 0.5\angle{0°}$. These results indicate an improvement in line protection efficiency, particularly in terms of instantaneous coverage with the phase variation.

When $\text{SIR}_{R,q}$ magnitude was further reduced to 0.05 (Fig. 4c), the same characteristics described previously were observed, with 98.2% of line coverage (instantaneous coverage of 96.4%) for $\text{SIR}_{R,q}$ equal to $0.05\angle{-20°}$ and $0.05\angle{20°}$, and 98.5% (instantaneous coverage of 97%) for $0.05\angle{0°}$. In other words, the stronger the remote source, the larger the 87LTQ percentage of instantaneous coverage for the local terminal. However, it is important to note that we are considering only a short-line transmission profile without the use of pickup thresholds, which may influence cases with high resistances that reduce the value of the negative-sequence current. Even so, this function exhibits advantageous characteristics, such as independence from the system load, fault type (as long as it is asymmetric), and fault resistance.

B. Computational Analysis of Transients

The computational analysis of transients considered double-line faults (BC) with 100 Ω of fault resistance, located at 20% and 80% of the line length. Furthermore, for this case, $\text{SIR}_{L,q} = 0.1$ and $\text{SIR}_{R,q} = 1.0\angle{-20°}$ were considered. Fig. 5 presents the obtained results.

It is worth mentioning that both evaluated cases, presented in Figs. 5a and 5b, lie on the blue curve (corresponding to $\text{SIR}_{R,q} = 1.0\angle{-20°}$) in Fig. 4a. However, their trajectories over time exhibit a slight deviation, mainly due to phasor estimation errors. Despite this, the trajectory is established at a specific point. In Fig. 5a, the fault occurs closer to the local terminal, while in Fig. 5b, the fault is near the restraining zone.

As aforementioned, it is observed that the fault occurred in circuit 1, since Γ_{Q1L} moves out of the restraining zone. Another relevant point for analysis is that Γ_{Q2L} tends to approach the origin (0,0), because $|\bar{I}_{L1Q}| \gg |\bar{I}_{L2Q}|$. This behavior suggests that negative-sequence current in circuit 1 has a significantly greater contribution than in circuit 2.

One can say that the 87LTQ element has a theoretical infinite sensitivity to load current and fault resistances. In other words, there is always a Γ_{1Q} whenever an asymmetric fault

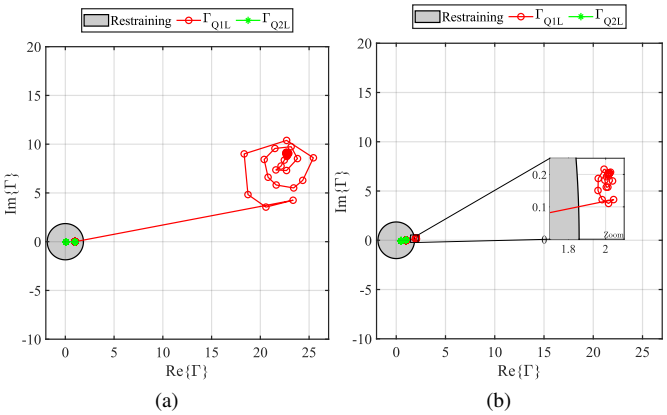

Fig. 5: Transient analysis of the alpha-plane with h: (a) 20%, (b) 80%.

takes place. Nonetheless, the proposed function performance is limited by the pickup threshold (I_{pk}) and also the slope K, which is related to the restraining region radius.

C. Experimental Analysis

In order to experimentally compare the proposed algorithm with widespread protection functions, the proposed negative sequence cross-differential protection was implemented in a commercially available IED, that provides an embedded environment for algorithms implementation, allowing access for its internal analog and digital quantities. Also, the implemented algorithm shares the same processing interval of native protection functions, in a way that makes it desirable for algorithms comparison. It is noteworthy to point out that for the analysis, the proposed algorithm was compared with IEDs phasor-based distance element (PH21). To ensure the algorithm dependability, if the alpha-plane coefficient was outside the restraining characteristic defined in (10) and each current magnitude was above an user-specified threshold, for half-cycle consecutive samples, a trip command should be issued.

For the experimental tests, a real model of a 230 kV system from Brazilian Interconnected System with a 99 km long double-circuit transmission line was evaluated. The line parameters are described in Table III.

TABLE III: Line parameters

Impedance	Value (Ω)
Z_{L0}	$163.96\angle 77.29°$
Z_{L1}	$46.75\angle 83.73°$
Z_{L2}	$46.75\angle 83.73°$
Z_{M0}	$107.98\angle 73.33°$

In which Z_{L0}, Z_{L1} and Z_{L2} stand for zero-, positive- and negative-sequence circuit self-impedance, wehereas Z_{M0} stands for zero-sequence mutual coupling impedance.

Regarding instrument transformers, 2000-5 CTs were modeled according to [11] and CCVTs were modeled by means of Haefely 230 implementation, considering parameters described in [12]. The testing methodology consisted in a modification of an ATPDraw base file in multiple files with fault parameters variation. After simulation, the waveforms were converted to COMTRADE files, which were injected into protective relay test sets connected to the commercial

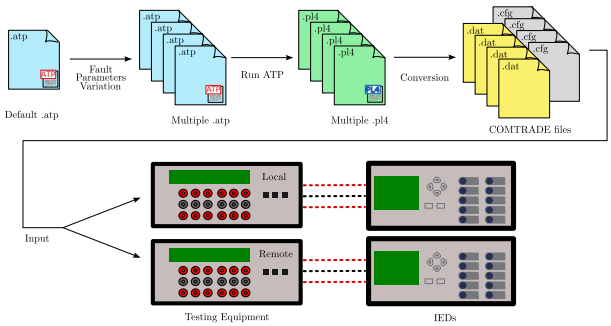

Fig. 6: Testing procedure.

IEDs. The proposed analysis considered the digital signals reported by the IEDs. Since the system available represents a real modeled system, only fault parameters were varied, in order to preserve the characteristics of the system. For the variation of fault parameters, changes were made to the fault location (h) and the fault resistance (R_f). The testing setup is illustrated in Fig. 6. Furthermore, relay parameterization considered PH21 with mho and quadrilateral characteristics for ground elements, and mho characteristics for phase elements, both with a 80% reach setting [13].

1) Sensitivity Analysis for variation in fault location and fault resistance for a single-line-to-ground fault: The first sensitivity analysis considered a fault location and fault resistance variation for a single-line-to-ground fault. To do so, fault location was varied from 2% to 98% in steps of 1%.

Fig. 7 presents the results for a bolted single-line-to-ground fault on phase A. From Fig. 7a, we can see that local element of PH21 operated for faults between 2% and 74%, whereas the remote terminal of such element operated for faults between 25% and 98%. Therefore, instantaneous non-communication operation by simultaneous first zone tripping occurred for faults between 25% and 74% (*i.e.,* a total instantaneous operation coverage for 49% of the line). Also, we can see that tripping times increased from approximately 10 ms to 20 ms as the fault moved away from the analyzed terminal. Considering the proposed algorithm, presented in Fig. 7b, we can see that local element operated for faults between 2% and 78%, whereas the remote terminal operated for faults between 5% and 98%. Therefore, instantaneous non-communication operation by simultaneous tripping occurred for faults between 5% and 78%, with a 73% coverage, higher in 24% of the line length when compared with PH21. From the analysis of the tripping time, we can see that the proposed algorithm operated about 12 ms for most of the cases.

Fig. 8 presents the results for a 150 Ω single-line-to-ground fault on phase A. From Fig. 8a, we can see that local element of PH21 operated for faults between 2% and 45%, whereas the remote terminal of such element operated for faults between 75% and 98%. Also, we can see that tripping times remained around 25 ms for most cases, with tripping times increasing as the fault moves away from the analyzed terminal. From this result, we can also see that a blind-zone between 46% and 74% occurred so that PH21 does not provide instantaneous operation of both line terminals at the same time for any location. Conversely, considering the proposed algorithm, presented in Fig. 8b, we can see that local element operated for faults between 2% and 78%, whereas the remote terminal operated for faults between 29% and 98%. Therefore, instantaneous non-communication operation by simultaneous tripping occurred for faults between 29% and 78%, with a 49% coverage. From the analysis of the tripping time, we can see that the proposed algorithm operated around 20 ms for most of the cases, for both local and remote terminals, which is directly related to the values of I_{pk} and K.

2) Sensitivity Analysis for variation in fault location and fault resistance for a double-line fault: The second sensitivity analysis considered a fault location and fault resistance variation for a double-line fault taking phases B an C. To do

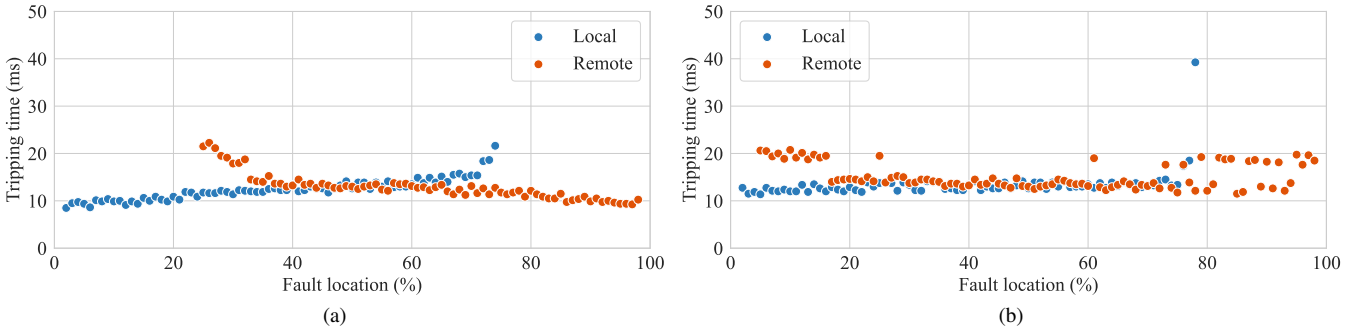

(a) (b)

Fig. 7: Sensitivity analysis for a single-line-to-ground fault with $R_f = 0\ \Omega$: (a) PH21, (b) 87LTQ.

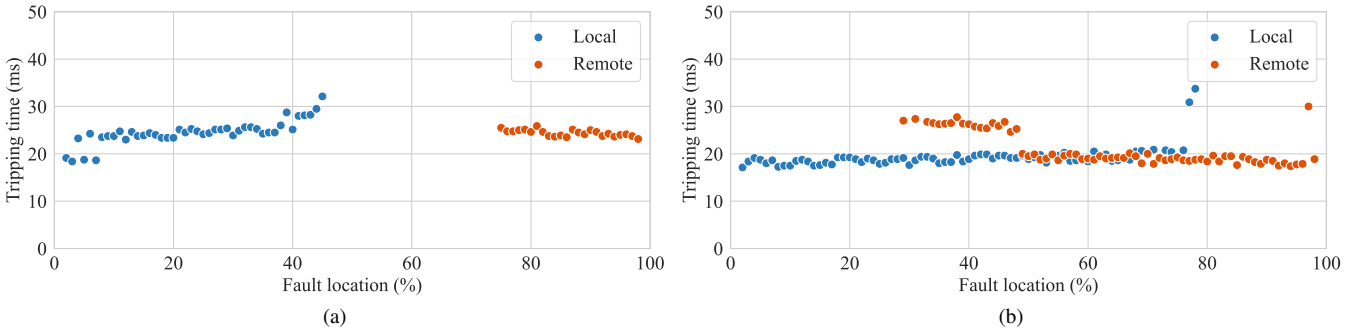

(a) (b)

Fig. 8: Sensitivity analysis for a single-line-to-ground fault with $R_f = 150\ \Omega$: (a) PH21, (b) 87LTQ.

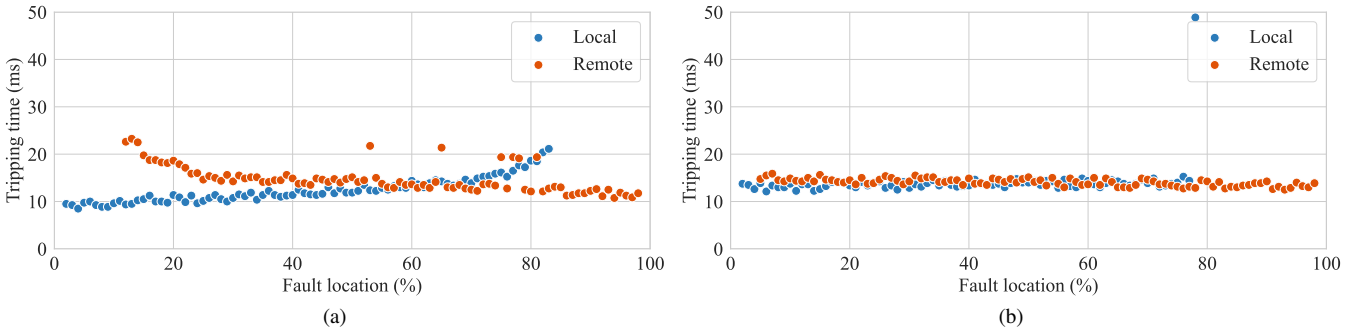

(a) (b)

Fig. 9: Sensitivity analysis for a double-line fault with $R_f = 0\ \Omega$: (a) PH21, (b) 87LTQ.

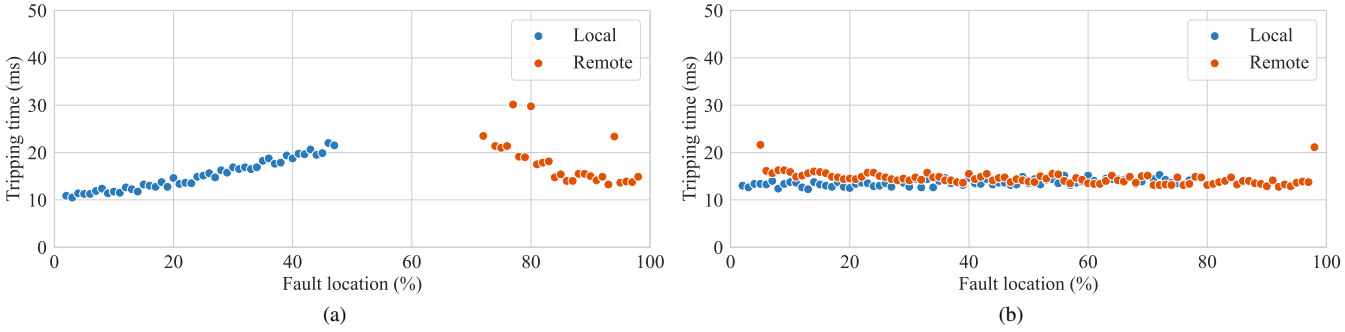

(a) (b)

Fig. 10: Sensitivity analysis for a double-line fault with $R_f = 30\ \Omega$: (a) PH21, (b) 87LTQ.

so, fault location was also varied from 2% to 98% in steps of 1%.

Fig. 9 presents the results for a bolted double-line fault on phases B and C. From Fig. 9a, we can see that local element

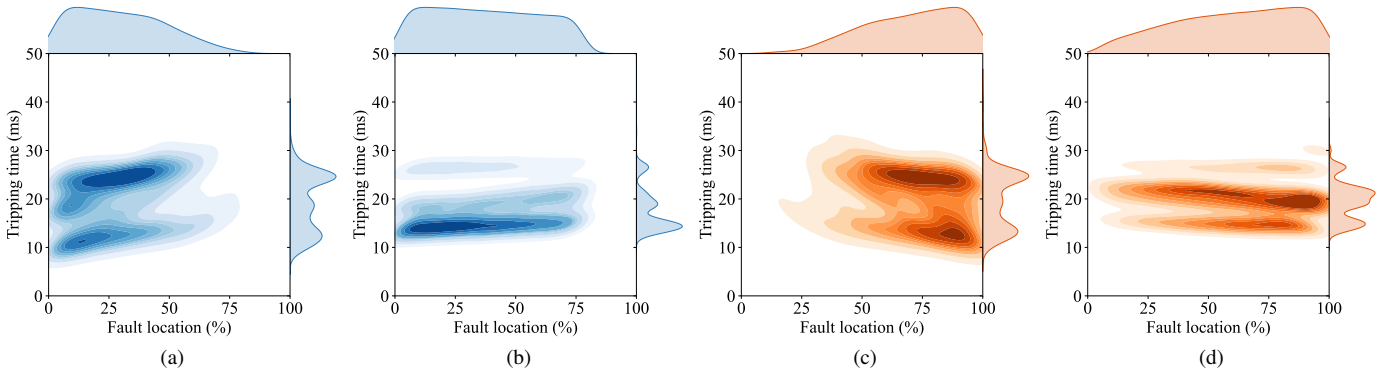

Fig. 11: Sensitivity analysis for a double-line fault : (a) Local terminal - PH21, (b) Local terminal - 87LTQ, (c) Remote terminal - PH21, (d) Remote terminal - 87LTQ.

of PH21 operated for faults between 2% and 83%, whereas the remote terminal of such element operated for faults between 12% and 98%. Therefore, instantaneous non-communication operation by simultaneous first zone tripping occurred for faults between 12% and 83%, with a 71% coverage, which is higher than the previous case. We can also see that tripping times increased from approximately 10 ms to 20 ms as the fault moved away from the analyzed terminal. Considering the proposed algorithm, presented in Fig. 9b, we can see that local element operated for faults between 2% and 77%, whereas the remote terminal operated for faults between 5% and 98%. Therefore, instantaneous non-communication operation by simultaneous tripping occurred for faults between 5% and 78%, with a 73% coverage, higher in 2% of the line length when compared with PH21. From the analysis of the tripping time, we can see that the proposed algorithm operated around 14 ms for most of the cases, with a more stable tripping time.

Fig. 10 results for a 30 Ω double-line fault. From Fig. 10a, we can see that local element of distance protection operated for faults between 2% and 47%, whereas the remote terminal of such element operated for faults between 72% and 98%. Also, we can see that tripping times increased from about 10 ms to 20 ms as the fault moved away from the analyzed terminal. From this result, we can also see a blind-zone, between 48% and 71% of the line so that PH21 does not operate instantaneously for any terminal within these percentage of the line. Considering the proposed algorithm, presented in Fig. 10b, we can see that the local element operated for faults between 2% and 77%, whereas the remote terminal operated for faults between 5% and 98%. Therefore, instantaneous non-communication operation by simultaneous tripping occurred for faults between 5% and 77%, with a 72% coverage. From the analysis of the tripping time, we can see that the proposed algorithm operated around 14 ms for most of the cases.

3) Statistical analysis for fault location and fault resistance variation: The third sensitivity analysis considered a fault location and fault resistance variation for single-line-to-ground and double-line faults applied in the analyzed transmission line. To do so, fault location was varied from 2% to 98% in steps of 1%. For each fault location, fault resistance was varied from 0 Ω to 400 Ω, in steps of 10 Ω, therefore with 3977 fault cases for each fault type, resulting 7954 fault playbacks in each IED.

Fig. 11 presents a statistical analysis by means of Kernel Density Estimation for the tripping times and fault location for each protection element [14], [15].

Figs 11a and 11b present the behavior for local elements of PH21 (1332 operations) and the proposed algorithm (5640 operations) respectively. From the fault location distribution, depicted at the top of each figure, we can see that PH21 operated for cases with higher fault resistance close to the analyzed terminal, since the fault location distribution presented a decaying behavior, which is related to the reach reduction caused by fault resistance. On the other hand, the proposed algorithm presented a more flat fault location distribution, which illustrates that it is less sensitive to fault resistance. Regarding tripping time distribution, located at the right side of each figure, we can see that distance element tripping times were more located close to 30 ms, whereas the proposed algorithm tripping times range between 10 ms and 20 ms.

Figs. 11c and 11d present the behavior for remote elements of PH21 (1114 operations) and the proposed algorithm (5515 operations) respectively. For PH21 we can see similar behavior presented by local terminal, whereas by the proposed algorithm, we can see that they operated for almost the entire length of the transmission line, but the number of operation was reduced due to the pickup threshold limitations. Considering tripping times, we can see that distance protection operated typically near 30 ms, whereas the proposed algorithm operated typically between 20 ms and 30 ms, which can be explained by source strength difference.

V. Conclusions

This paper proposed a new alpha plane-based negative sequence cross-differential protection algorithm for double-circuit transmission lines. To do so, computational and experimental evaluations were performed in system modeled in ATPDraw.

From the fault trajectories, we found that the proposed protection will exhibit circular arc trajectories with varying

fault locations and a line with real values only when the SIR values are real (*i.e.,* when the system is ideally homogenous). From the experimental results, we can see how the proposed algorithm had a better performance when compared to PH21 for assymetrical faults, specially in the case of high fault resistance.

Therefore, the proposed algorithm arises as a promising solution to complement double-circuit transmission line protection. Neverthless, for the method to work properly, both circuits must be in service, with both line terminals closed, so an additional algorithm that detects when one of the circuits of the double-circuit transmission line is open is necessary to block the negative-sequence cross-differential algorithm. That is the why the proposed algorithm must be used along with other protection functions to guarantee dependability of the protection scheme as a whole. This research is ongoing, such that further improvements will be presented in a future publication.

REFERENCES

[1] M. Sanaye-Pasand and P. Jafarian, "Adaptive protection of parallel transmission lines using combined cross-differential and impedance-based techniques," *IEEE Transactions on Power Delivery*, vol. 26, no. 3, pp. 1829–1840, 2011.

[2] A. Apostolov, D. Tholomier, S. Sambasivan, and S. Richards, "Protection of double circuit transmission lines," in *2007 60th Annual conference for protective relay engineers*. IEEE, 2007, pp. 85–101.

[3] V. Serpa, T. Honorato, K. Silva, and E. Neves, "Experimental evaluation of cross-differential protection applied on double-circuit transmission lines protection (in portuguese)," in *18th IberoAmerican Regional Meeting from CIGRE, Foz do Iguaçu, Brazil, 2019*, 2019.

[4] V. R. Serpa, T. R. Honorato, J. V. L. Pedrosa, K. M. Silva, and F. V. Lopes, "Experimental evaluation of cross-differential protection applied to series-compensated double-circuit lines," in *15th International Conference on Developments in Power System Protection (DPSP 2020)*. IET, 2020, pp. 1–6.

[5] Q. Wang, X. Dong, Z. Bo, B. Caunce, A. Apostolov, and D. Tholomier, "Cross differential protection of double lines based on supper-imposed current," in *CIRED 2005-18th International Conference and Exhibition on Electricity Distribution*. IET, 2005, pp. 1–4.

[6] H. Altuve, G. Benmouyal, J. Roberts, and D. A. Tziouvaras, "Transmission line differential protection with an enhanced characteristic," 2004.

[7] D. Tziouvaras, H. Altuve, G. Benmouyal, and J. Roberts, "The effect of multiprinciple line protection on dependability and security," *Schweitzer Engineering Laboratories Inc., Pullman, WA, Tech. Rep*, 2001.

[8] V. R. Serpa, T. R. Honorato, and K. M. Silva, "Evaluation of cross-differential protection applied to double-circuit transmission lines under inter-circuit faults," *Simpósio Brasileiro de Sistemas Elétricos-SBSE*, vol. 1, no. 1, 2020.

[9] C. L. Fortescue, "Method of symmetrical co-ordinates applied to the solution of polyphase networks," *Transactions of the American Institute of Electrical Engineers*, vol. 37, no. 2, pp. 1027–1140, 1918.

[10] M. J. Thompson and A. Somani, "A tutorial on calculating source impedance ratios for determining line length," in *2015 68th Annual Conference for Protective Relay Engineers*. IEEE, 2015, pp. 833–841.

[11] E. Pajuelo, G. Ramakrishna, and M. Sachdev, "Phasor estimation technique to reduce the impact of coupling capacitor voltage transformer transients," *IET generation, transmission & distribution*, vol. 2, no. 4, pp. 588–599, 2008.

[12] A. V. Carvalho Jr, "Transient interaction between capacitive potential transformers and transmission lines: A contribution to minimize faults," Master's thesis, Federal University of Pernambuco, Recife, Brazil, 2008.

[13] F. Calero, A. Guzmán, and G. Benmouyal, "Adaptive phase and ground quadrilateral distance elements," in *proceedings of the 36th Annual Western Protective Relay Conference, Spokane, WA*, 2009, p. 43.

[14] M. Rosenblatt, "Remarks on Some Nonparametric Estimates of a Density Function," *The Annals of Mathematical Statistics*, vol. 27, no. 3, pp. 832 – 837, 1956. [Online]. Available: https://doi.org/10.1214/aoms/1177728190

[15] E. Parzen, "On Estimation of a Probability Density Function and Mode," *The Annals of Mathematical Statistics*, vol. 33, no. 3, pp. 1065 – 1076, 1962. [Online]. Available: https://doi.org/10.1214/aoms/1177704472